International Journal of Minerals, Metallurgy and Materials
Volume 27, Number 3, March 2020, Page 292
https://doi.org/10.1007/s12613-019-1856-z

Study on the mechanical activation of malachite and the leaching of complex copper ore in the Luanshya mining area, Zambia

Gai-rong Wang[1,2], *Hong-ying Yang*[1,2], *Yuan-yuan Liu*[3], *Lin-lin Tong*[1,2], *and Ali Auwalu*[1,2]

1) Key Laboratory for Ecological Metallurgy of Multimetallic Mineral (Ministry of Education), Northeastern University, Shenyang 110819, China
2) School of Metallurgy, Northeastern University, Shenyang 110819, China
3) CNMC Luanshya Copper Mines Plc (CLM), Independence Avenue, Luanshya City 90456, Zambia
(Received: 19 March 2019; revised: 15 May 2019; accepted: 3 June 2019)

Abstract: Mechanical activation (MA) of malachite was carried out by dry planetary grinding (DPG) and wet Isa grinding (WIG) methods. When the rotational speed was increased to 400 r/min in DPG, the specific surface area of malachite reached the maximum and the particle size reached the minimum of 0.7–100 μm. Agglomeration occurred between mineral particles when the rotational speed was increased to 580 r/min in DPG. However, no agglomeration was observed among particles with sizes 0.4–3 μm in WIG. X-ray diffraction analysis showed that, at a 580 r/min rotational speed in DPG, the amorphization degree of malachite was 53.12%, whereas that in WIG was 71.40%, indicating that MA led to amorphization and distortion of crystal structures. In addition, in the Fourier transform infrared (FT-IR) spectra of activated malachite, the bands associated with –OH, $CO_3^{2-}$and metal lattice vibrations of Cu–O and Cu–OH were weakened, and a new H–O–H bending mode and peaks of gaseous CO_2 appeared, indicating that MA decreased the band energy, enhanced dihydroxylation, and increased the chemical reactivity of the malachite. Furthermore, the leaching behavior of copper ore was greatly improved by MA.

Keywords: malachite; mechanical activation; crystal structure; copper ore; Zambia

1. Introduction

According to their proportion of oxide minerals and sulfide minerals, copper ores can be categorized as sulfide ores containing less than 10wt% copper oxide, mixed ores containing 10wt%–30wt% copper oxide, or oxide ores containing more than 30wt% copper oxide [1]. With the continuous consumption of copper sulfide ores, the development and utilization of copper oxide ores is becoming increasingly important. Malachite ($Cu_2(OH)_2CO_3$) is one of the most important minerals in copper oxide ores. At present, complex copper oxide ores rich in malachite are used to produce copper through various hydrometallurgical processes, including acid leaching [2–4], ammonia leaching [5–7], and biological leaching [8]. Such hydrometallurgical processes can achieve substantial copper leaching rates but with the disadvantages of long leaching times, the generation of environmental pollution, and high consumption of reagents.

Overcoming the aforementioned shortcomings associated with leaching malachite-rich complex copper oxide ores necessitates pretreatment before leaching. At present, the common pretreatment methods are mechanical activation (MA) and electromagnetic wave activation (microwaves, ultrasound, etc.) [9]. MA is a process that can increase the internal energy and reaction activity of minerals through mechanical forces such as friction, impact, collision, and shear, which lead to lattice distortion, lattice defects, and amorphization [10–11]. MA leads to changes in certain properties of mineral particles, such as an increase in their specific surface area and structural disorder [12], an enhancement of strain [13], an increase in amorphization [10], alteration of their microtopography [14], and the formation of new phases more amenable to being leached [15]. Recent studies have shown that the process of MA generally includes two grinding modes: dry and wet grinding modes. The dry grinding mode mainly produces the milling effects of rubbing and

Corresponding author: Hong-ying Yang E-mail: yanghy@smm.neu.edu.cn

crushing that cannot reduce small particles to finer particles [16]. However, the wet grinding mode relies on high-energy agitation to effectively drive small grinding media and form a large number of compressed rotating media layers that can create pressure and torsional forces. These two forces are much more effective for grinding small particles than the rubbing and crushing forces generated by the dry grinding mode [17]. For example, the X-ray diffraction (XRD) analysis of activated realgar revealed broadened diffraction peaks with diminished intensity after activation; in addition, the peak of an obviously amorphous phase appeared at 2θ = 16° [18]. In addition, Kleiv and Thornhill [19] reported that the specific surface area of olivine was substantially increased by MA, and that it was higher after combined activation by dry and wet modes (64.44 ± 2.13 m^2/g) than after dry activation alone (26.28 ± 1.28 m^2/g). Tkáčová and Stevulová [20] investigated the effects of activation of carbonates and quartz by dry and wet grinding in air and aqueous environments. Their results showed that the content of the X-ray-amorphous phase in the ground material increased with increasing grinding work although it remained unaffected by the grinding environment; in addition, the use of an aqueous environment resulted only in an enlarged specific surface area of the ground products. Dry grinding experiments involving quartz-based malachite mixtures were carried out for different grinding times by Tunç and Yildiz [21]. Their results showed obvious effects of the MA phenomenon, such as broadening of the XRD peaks, a reduction in XRD peak intensity, a shift of the XRD angles, and the generation of amorphous silicon. However, research on the characterization of activated malachite with regard to specific phases and crystal structures as well as the leaching effect have rarely been reported.

In this work, the mechanism of MA and its effect on the physicochemical properties of malachite by dry planetary grinding (DPG) and wet Isa grinding (WIG) were investigated using XRD, scanning electron microscopy with energy-dispersive X-ray spectroscopy (SEM-EDS), and Fourier transform infrared (FT-IR) spectroscopy. The results of this study not only reveal a convenient method for obtaining malachite but also provide a theoretical basis and significant guidance for the leaching of malachite-rich complex copper oxide ores.

2. Experimental

2.1. Materials

The elements of malachite samples were analyzed by X-ray fluorescence (XRF) spectroscopy; the results are presented in Table 1. The main elements were Cu, Co, Fe, and Si. The quantitative analysis indicated that the sample contained 53.5wt% Cu with 5.3wt% C. Fig. 1 shows the XRD pattern, confirming the presence of malachite. In addition, the complex copper ores rich in malachite were obtained by open-pit mining from the Luanshya mining area, Zambia. The main Cu-bearing minerals were malachite, chrysocolla, and pseudo-malachite [22].

Table 1. XRF analysis results for the malachite sample wt%

CuO	Co_2O_3	Fe_2O_3	SiO_2	HfO_2	MgO	Al_2O_3	P_2O_5	MnO	Others
91.23	3.99	1.47	1.38	0.49	0.38	0.34	0.32	0.18	0.22

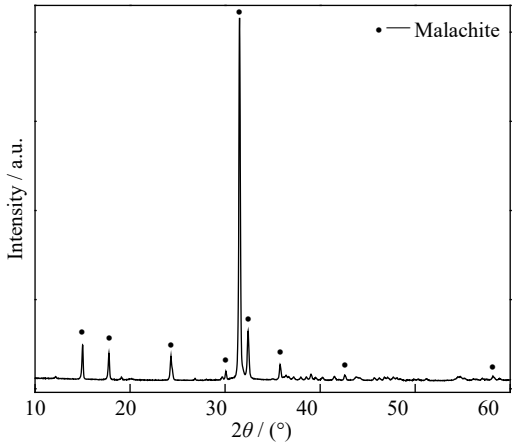

Fig. 1. XRD pattern of the malachite sample.

2.2. Mechanical activation

In this study, the MA of malachite was performed in a dry planetary mill (QM3SP2 Planetary mill, China) and a wet Isa mill (ALC-1.5L mill, China). The dry planetary milling was conducted as follows: 15 g of malachite sample was combined with 180 g of zirconia grinding balls, where the mass ratio of grinding balls 5, 10, and 20 mm diameter was 3:4:5, respectively. The samples were mechanically activated at different rotation speeds from 200 to 580 r/min for 10 min (580 r/min was the rated speed). The conditions used for the wet Isa milling were as follows: 100 g of malachite sample and 3600 g of ceramic grinding balls (1 mm in diameter), and 800 mL of water were combined, and the samples were mechanically activated at 2000 r/min for 10 min.

2.3. Characterization

The Brunauer–Emmett–Teller (BET) specific surface area was determined via the low-temperature nitrogen adsorption method using a NOVA 1200e surface area and pore size analyzer. The values were calculated according to the BET theory. The micro-morphologies of the particles were characterized by SEM using an electron microscope (Shimadzu SSX-550) equipped with an EDS detector. The particle size distribution (PSD) was estimated using a laser particle sizer (Malvern Instruments Mastersizer 2000). The crystal structure analysis of malachite samples was conducted through XRD (SmartLab) analysis. The measurement conditions were as follows: Cu $K\alpha_1$ radiation, curved height 0.42, scan range $10° \leq 2\theta \leq 40°$, step scan with a speed of 1°/min, U = 40 kV, I = 200 mA, T = 23.0°C. The chemical bonds of malachite samples were evaluated using FT-IR spectroscopy (VERTEX70) over the mid-infrared spectral range from 450 to 3500 cm^{-1}.

2.4. Leaching tests

In this experiment, the leaching of nonactivated and activated copper ores rich in malachite were carried out in sulfuric acid. The leaching conditions were as follows: sulfuric acid 0.5 mol/L, temperature 30°C, solid-to-liquid ratio 50 g/L, stirring speed 300 r/min, and leaching time 120 min.

3. Results and discussion

3.1. Specific surface area

The BET specific surface area (S_{BET}) of nonactivated malachite samples and samples mechanically activated by different grinding methods are presented in Fig. 2. Compared with the BET specific surface area of the nonactivated malachite, that of activated malachite was greater, indicating that the particles were further refined. For the malachite activated by DPG, with increasing rotational speed, the BET specific surface area increased, reaching a maximum of 14.158 m^2/g at a rotation speed of 400 r/min, which is 1.43 times greater than the BET surface area of the nonactivated sample. However, the BET specific surface area of malachite decreased unexpectedly when the rotational speed was increased to 580 r/min. The mineral samples adhered to the balls and sunk to the bottom at the highest grinding speed (580 r/min) in DPG, leading to agglomeration between the small mineral particles and to adsorption of the small particles onto the surface of the large particles [23]. In addition, a BET specific surface area of 25.280 m^2/g was achieved in WIG, which is 2.56 times greater than that of the nonactivated sample. Although the rotational speed (2000 r/min) of the Isa mill was almost 3.45 times greater than that of the planetary mill (580 r/min), no agglomeration was observed between particles and the grains were much finer in the sample subjected to WIG. This result was attributed to the high-strength wet agitation of the Isa mill effectively dispersing the particles rather than inducing their agglomeration [24].

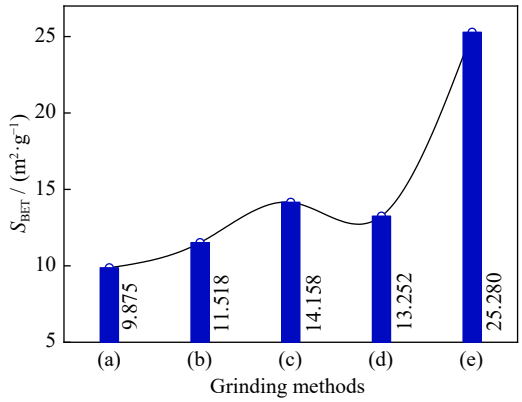

Fig. 2. BET specific surface area of malachite samples activated by different grinding methods: (a) nonactivated; (b) 200 r/min in DPG; (c) 400 r/min in DPG; (d) 580 r/min in DPG; (e) WIG.

3.2. Particle micromorphology and size distribution

3.2.1. Particle micromorphology

Fig. 3 shows the SEM-EDS images of malachite samples activated by different grinding methods. As shown in Fig. 3(a), the nonactivated malachite consisted of compact particles with different sizes and patterns. The patterns were irregular in shape, with a clear rhombus angle and smooth surface. Additionally, the uneven sizes of the malachite particles indicated that they lacked homogeneity. When the DPG rotational speed was increased to 200 r/min, the morphological features of the malachite samples were obviously changed. These changes were reflected by a sharp decrease in particle size and a roughened surface, as shown in Fig. 3(b). As the rotational speed was increased to 580 r/min in DPG, the malachite samples were substantially transformed from angular shapes to sphere-like structures. Nevertheless, serious agglomeration of the malachite particles is appeared at rotational speed of 580 r/min in Fig. 3(c), consistent with the results of the BET specific surface area shown in Fig. 2(d).

Compared with the particles of malachite samples activated by DPG, those of the samples activated by WIG were extremely small and dispersed uniformly, with no agglomeration (Fig. 3(d)). This phenomenon is attributed to the fact

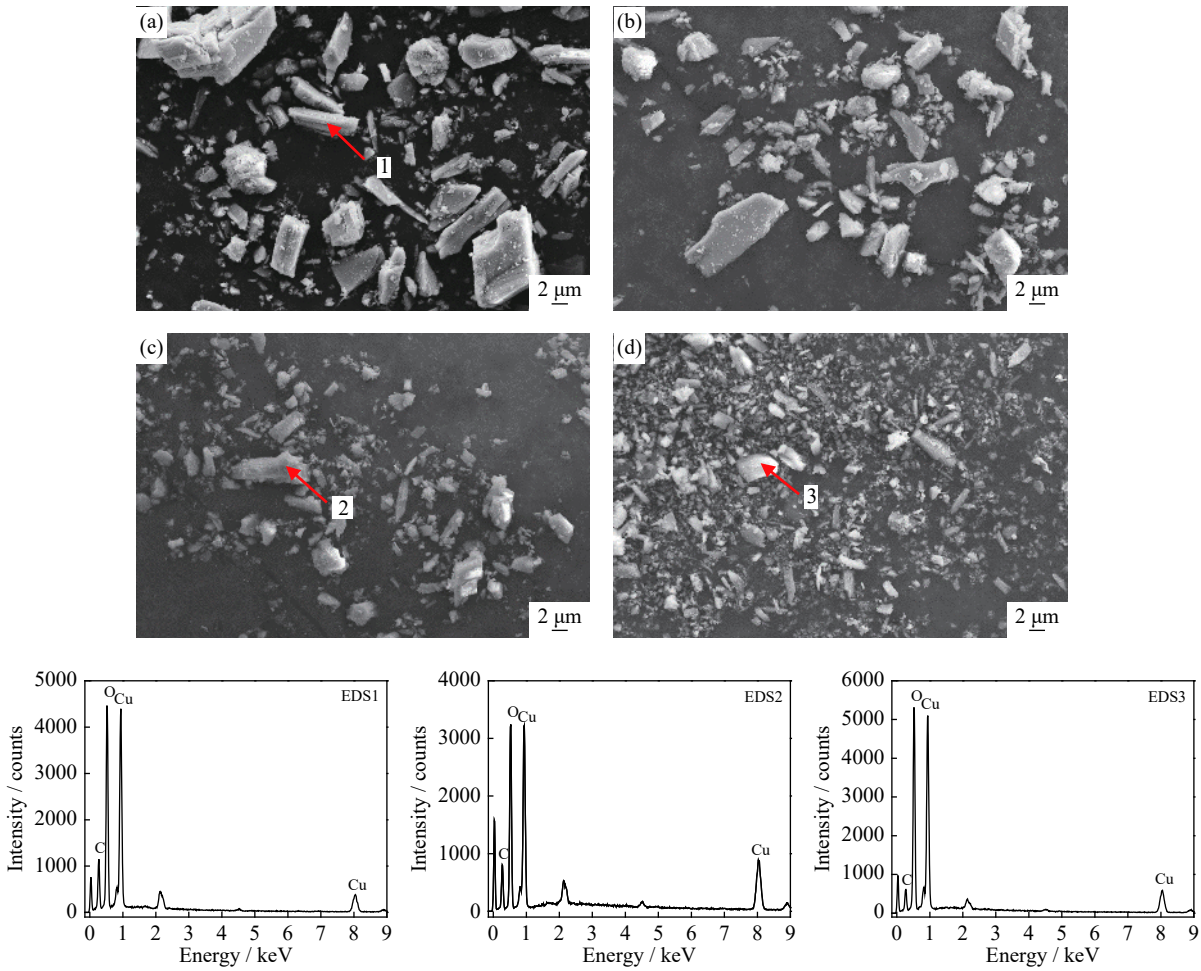

Fig. 3. SEM images and EDS analyses of malachite samples activated by different grinding methods: (a) nonactivated; (b) 200 r/min in DPG; (c) 580 r/min in DPG; (d) WIG. Spectra EDS1, EDS2, and EDS3 correspond to points 1, 2, and 3, respectively, in SEM micrographs.

that the high-strength wet agitation in WIG paves no way for the particles to mutually agglomerate. In addition, the EDS spectrogram reveals that no phase transformation of malachite occurred during either DPG or WIG.

3.2.2. Particle size distribution

The PSD curves of the malachite samples activated by different grinding methods are presented in Fig. 4. The PSD curve of the nonactivated malachite shows a single, broad peak corresponding to a size range from 0.5 to 300 μm. However, the PSD curves for the samples activated by DPG show broad distributions with multiple peaks. When the rotational speed was 200 r/min, the particle size range was 0.4–250 μm. As the rotational speed was increased to 400 r/min, the particle size range still was 0.4–250 μm while the distribution of large particle decreased. As the rotational speed was increased further to 580 r/min, the particle size range increased to 0.4–500 μm. The abnormal PSD of the sample activated by DPG at 580 r/min is attributed to the

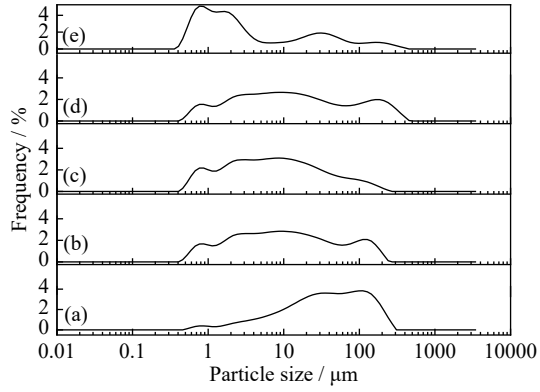

Fig. 4. Particle size distributions of malachite samples activated by different grinding methods: (a) nonactivated; (b) 200 r/min in DPG; (c) 400 r/min in DPG; (d) 580 r/min in DPG; (e) WIG.

higher grinding speed causing the mineral samples adhere to the balls and sink to the bottom, leading to agglomeration among the small mineral particles and to adsorption of the

small particles onto the surface of the large particles, which led to larger particles. This result is consistent with the analysis of the BET specific surface area and the aforementioned particle micromorphology.

The results in Fig. 4 also show that the peak in the PSD curve of the sample subjected to WIG was single and narrow, corresponding to small, 0.4–3 μm particles. This result differs substantially from the single peak in the curve of the nonactivated malachite sample, which contained large, 10–300 μm particles, indicating that the micro refinement effect of WIG was remarkable.

3.3. XRD crystal structure analysis

Fig. 5 represents the XRD patterns of malachite samples activated by different grinding methods. In addition, the corresponding crystal lattice parameters are presented in Table 2, which also includes the average apparent crystallite size D and the average maximum strain ε. The results in Table 2 indicate that the parameters a, b, c, V, and D gradually decreased as the rotational speed was increased to 400 r/min in DPG. At this speed, the parameters a, b, c, V, and D reached their minimum values, in accordance with the maximum specific surface area as well as the smallest particle size, as previously discussed. However, when the rotational speed was increased to 580 r/min, the values of parameters a, b, c, V, and D did not continue their previous decreasing trend but instead increased because of agglomeration of the mineral particles. Unexpectedly, the average maximum strain ε gradually increased from 0.022% for the nonactivated sample to 0.034% for the sample activated at 580 r/min, indicating that greater surface energy was produced at high rotational speeds in DPG, leading to a continuous increase in the particle lattice distortion. Moreover, the smallest values of parameters a, c, V, and D and the highest average maximum strain ε of 0.045% were achieved in WIG, which indicates that the effects of reducing the particle crystallinity and increasing the amorphization in WIG were far more significant than those in DPG.

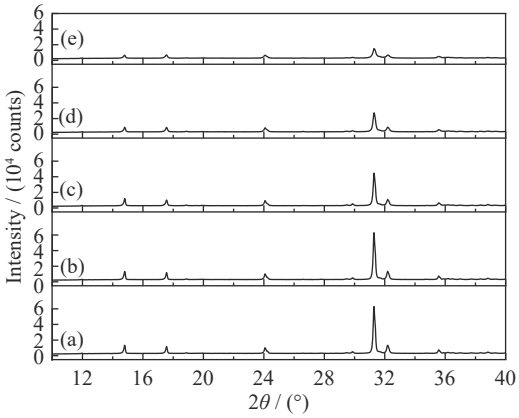

Fig. 5. XRD patterns of malachite samples activated by different grinding methods: (a) nonactivated; (b) 200 r/min in DPG; (c) 400 r/min in DPG; (d) 580 r/min in DPG; (e) WIG.

The XRD patterns in Fig. 5 clearly show that the XRD diffraction peak characteristics changed, but no phase transition was observed for the malachite samples activated by the different grinding methods. With increasing rotational speed in DPG, the XRD diffraction peaks of the activated samples generally broadened and their intensities decreased. This phenomenon was more evident in WIG, indicating that the distortion of the crystal structure and increase in the amorphization degree in WIG were more obvious than those in DPG. Additionally, the amorphization degree of malachite was calculated by the equation [25–26].

Fig. 6 shows the amorphization degrees of malachite activated by different grinding methods. These results indicate that the amorphization degrees of malachite increased gradually with increasing rotational speed during DPG. When the rotational speed was at 580 r/min in DPG, the amorphization degrees was 53.12%, whereas it was 71.40% in WIG, further indicating that the effect of MA by WIG was better than that by DPG.

3.4. FT-IR bonding analysis

Fig. 7 shows the FT-IR spectra of malachite samples activated by different grinding methods. The main absorption peaks in the FT-IR spectra are shown in Table 3 [27]. The spectra in Fig. 7 show that the intensive bands of malachite

Table 2. Crystallographic data and microstructural parameters of malachite samples activated by different grinding methods

Grinding methods	a / nm	b / nm	c / nm	β / (°)	V / nm^3	D / nm	ε / %
Nonactivated	0.95081	1.19644	0.32446	98.6251	0.36492	75.8	0.022
200 r·min^{-1} in DPG	0.95009	1.19615	0.32444	98.6933	0.36450	75.5	0.023
400 r·min^{-1} in DPG	0.94950	1.19581	0.32440	98.6181	0.36448	74.0	0.032
580 r·min^{-1} in DPG	0.95023	1.19572	0.32437	98.6946	0.36458	74.5	0.034
WIG	0.94901	1.19603	0.32435	98.6693	0.36436	59.9	0.045

Note: a, b, c, and β are unit-cell parameters; V is the unit-cell volume; D is the average apparent crystallite size; ε is the average maximum strain.

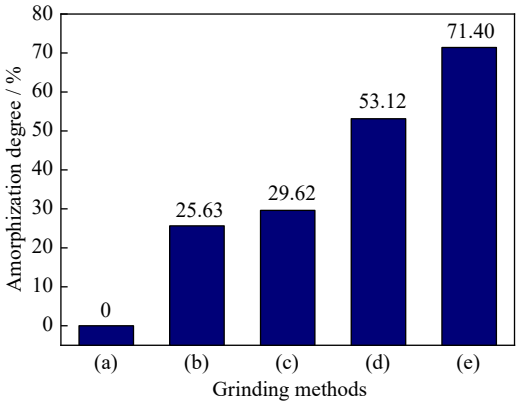

Fig. 6. Amorphization degrees of malachite samples activated by different grinding methods: (a) nonactivated; (b) 200 r/min in DPG; (c) 400 r/min in DPG; (d) 580 r/min in DPG; (e) WIG.

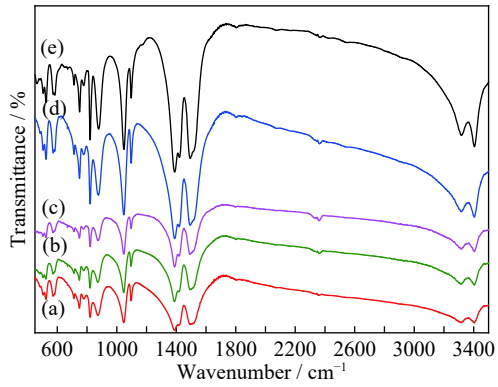

Fig. 7. FT-IR spectra of malachite samples activated by different grinding methods: (a) nonactivated; (b) 200 r/min in DPG; (c) 400 r/min in DPG; (d) 580 r/min in DPG; (e) WIG.

Table 3. Assignment of main absorption peaks in the infrared spectra of malachite samples

Grinding methods	ν(–OH)		δ(–OH)		$\nu_1(CO_3^{2-})$	$\nu_2(CO_3^{2-})$	$\nu_3(CO_3^{2-})$		$\nu_4(CO_3^{2-})$		Cu–O	Cu–OH
Nonactivated	3404.40	3313.24	1046.17	870.15	1096.27	819.73	1490.92	1386.69	748.04	712.03	569.98	523.52
200 r·min^{-1} in DPG	3404.49	3313.95	1046.85	872.77	1096.38	820.69	1491.35	1387.41	748.36	711.92	571.59	523.66
400 r·min^{-1} in DPG	3404.51	3314.68	1047.37	874.94	1096.40	820.92	1492.93	1388.36	748.86	712.09	571.24	524.13
580 r·min^{-1} in DP	3404.29	3315.77	1047.40	876.42	1096.77	821.01	1493.06	1389.24	749.34	712.40	572.52	524.41
WIG	3404.77	3317.31	1048.21	878.48	1096.92	821.17	1494.79	1389.58	750.25	712.86	583.76	524.89
Ref. [27]	3400	3320	1045	875	1095	820	1500	1400	748	710	570, 580	522

samples can be divided into four regions: 2800–3500 cm^{-1}, 1000–1500 cm^{-1}, 650–950 cm^{-1}, and <650 cm^{-1}, respectively. The centered bands of 3404.40, 3313.24, 1490.92, 1386.69, 1096.27, 1046.17, 819.73, 748.04, 712.03, 569.98, and 523.53 cm^{-1} were determined for a nonactivated malachite sample. However, some bands clearly changed in intensity, number, and position in the spectra of the activated samples, especially the sample activated by DPG at 580 r/min and that activated by WIG.

Fig. 7 shows that, as the rotational speed was increased to 400 r/min in DPG, the intensity and area of most of the absorption bands remained unchanged; however, the bands changed when the rotational speed was increased to 580 r/min. This observation was attributed to the activity of the mineral group being enhanced by the high-energy grinding, resulting in instability of the chemical bonds [28]. In addition, the intensity and area of the absorption bands increased substantially in the spectra of the sample activated by WIG compared with those in the spectra of the samples activated by DPG and the nonactivated samples. That is, the intensities of these bands were enhanced with increasing mineral disorder induced by grinding [29].

Goldsmith and Ross [27] have reported that the symmetrical vibration bands ν(–OH) groups appear at 3400 and 3320 cm^{-1} [27]. Tunç and Yildiz [21] mechanically activated impure malachite containing quartz and showed that the two –OH bands disappeared after activation. However, because of the high purity of malachite samples used in the present study, the two bands were still present at 3404.40 and 3313.24 cm^{-1} in the spectra of the activated malachite. We also found that the position of the –OH symmetrical vibration band remained almost unchanged in the spectra of DPG and WIG compared with that in the spectrum of the nonactivated malachite. Nevertheless, the positions of the two deformation vibration bands δ(–OH) at 1046.17 and 870.15 cm^{-1} slightly shifted to 1047.40 and 876.42 cm^{-1} in the spectrum of the sample activated by DPG at 580 r/min and to 1048.21 and 878.48 cm^{-1} in the spectrum of the sample activated by WIG, respectively. The center-shift of a band to higher frequency indicates a decrease in bond strength [30], suggesting that the –OH bond was weakened and that the free –OH content was increased. In the meantime, a new band attributed to the H–O–H bending mode gradually emerged at 1780.78 cm^{-1}, whereas no such band was observed in the spectrum of the nonactivated malachite [31], confirming that the structure of –OH was converted to free water via DPG and WIG [32]. Dehydroxylation is mediated by the interaction of two hydroxyl groups in a two-step proton transfer process that results in the formation of a water molecule and in a chemically bonded oxygen atom being left

in the form of a superoxide anion in the lattice. This reaction process is represented chemically in Eqs. (1) and (2) [33]:

$$OH^- \rightleftharpoons H^+ + O^{2-} \quad (1)$$

$$H^+ + OH^- \rightleftharpoons H_2O \quad (2)$$

The position of the symmetric stretching vibration $v_1(CO_3^{2-})$ at 1096.27 cm^{-1} was unchanged in the spectra of the samples activated by WIG and by DPG at 580 r/min. However, the unsymmetrical stretching vibrations $v_3(CO_3^{2-})$ shifted from 1386.69 and 1490.92 cm^{-1} in the spectra of nonactivated malachite to 1389.24 and 1493.06 cm^{-1} in the spectrum of the sample activated by DPG at 580 r/min and to 1389.58 and 1494.79 cm^{-1} in the spectrum of the sample activated by WIG [34]. In addition, the peak positions of the in-plane bending vibration $v_2(CO_3^{2-})$ at 819.73 cm^{-1} and the out-of-plane bending vibrations $v_4(CO_3^{2-})$ at 748.04 and 712.03 cm^{-1} shifted to 821.17 and to 750.25 and 712.86 cm^{-1} in the spectrum of the sample activated by WIG, respectively. The shift of a band center to higher frequencies indicates a decrease in bond strength [30]. Therefore, in combination with the results showing that the bands of CO_3^{2-} shifted to a higher position and the intensity increased, these results indicate that the absorption bands associated with CO_3^{2-} groups became gradually weaker. Moreover, we observed that a new band at 2366.71 cm^{-1} appeared in the spectra of the samples activated by DPG at 200, 400, and 580 r/min. The new band was attributed to gaseous CO_2, which was generated by decomposition of the atmosphere or CO_3^{2-} groups [35], as shown in Eq. (3). However, the new band of gaseous CO_2 nearly disappeared in the spectrum of the sample activated by WIG, leading to the presumption that the gaseous CO_2 was dissolved in water, as shown in Eq. (4):

$$Cu_2(OH)_2CO_3 = 2CuO + H_2O + CO_2\uparrow \quad (3)$$

$$CO_2 + H_2O = H_2CO_3 \quad (4)$$

The absorption bands of metal lattice vibrations of Cu–O and Cu–OH appear at 569.98 and 523.52 cm^{-1}, respectively. Their positions shifted to 572.52 and 524.41 cm^{-1} in the spectrum of the sample activated by DPG at 580 r/min and to 583.76 and 524.89 cm^{-1} in the spectrum of the sample activated by WIG, thereby demonstrating that the effect of MA was more remarkable in WIG than in DPG.

4. Leaching tests of samples activated by different grinding methods

Fig. 8 shows the leaching results for malachite-rich complex copper ore activated by different grinding methods and leached in sulfuric acid. The copper leaching rate obviously increased rapidly before 40 min and then increased slowly at 200 r/min in DPG, similar to the nonactivated ore. For the ores activated at 400 and 580 r/min, the leaching rate of copper increased rapidly before 10 min and then increased slowly. However, we found that the leaching rate of copper was extremely high before 2 min and then increased slowly in WIG. Although agglomerated particles were observed in the aforementioned analysis of the samples activated by DPG at 580 r/min, the leaching rate of ore activated at 580 r/min was slightly greater than that of the ore activated at 400 r/min, which is a consequence of a more distorted crystal structure and a greater amorphization degree of samples ground at higher speeds. Therefore, the order of copper leaching rate with respect to different grinding methods was achieved as follows: WIG > DPG > nonactivated, which well matches the results of the analyses of the specific surface area, PSD, and amorphization degree of the activated malachite.

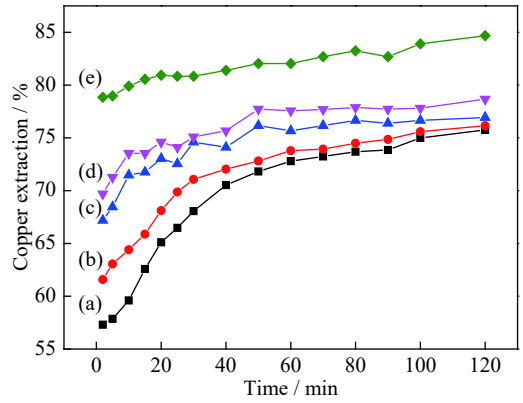

Fig. 8. Leaching results of malachite-rich copper oxide ore activated by different grinding methods and leached in sulfuric acid: (a) nonactivated; (b) 200 r/min in DPG; (c) 400 r/min in DPG; (d) 580 r/min in DPG; (e) WIG.

5. Conclusions

(1) The malachite samples were mechanically activated in DPG and WIG. The samples activated by WIG exhibited remarkable improvements in specific surface area, particle micromorphology, PSD, crystal structure, and chemical bonding.

(2) Agglomeration occurred between the mineral particles when the rotational speed was increased to 580 r/min in DPG. However, no particle agglomeration was observed for the samples activated by WIG, which exhibited a particle size of 0.4–3 μm.

(3) XRD analysis indicated that no phase transformation

of the activated malachite occurred in either DPG or WIG; however, the amorphization of the samples gradually changed. When the rotational speed was at 580 r/min in DPG, the amorphization degree of malachite was 53.12%, whereas it was 71.40% in WIG, showing that MA leads to amorphization and to distortion of the malachite crystal structure.

(4) In the FT-IR analysis, the absorption bands associated with –OH vibrations, CO_3^{2-} vibrations, and metal lattice vibrations of Cu–O and Cu–OH weakened and a new H–O–H bending mode as well as gaseous CO_2 appeared on the activated malachite minerals, indicating that MA can decrease the band energy, enhance dihydroxylation, and increase chemical reactivity, especially when conducted by WIG.

(5) The leaching properties of malachite-rich copper ore with respect to different grinding methods were greatly improved, especially the WIG, which well matches the results of the analyses of the specific surface area, PSD, and amorphization degree of the activated malachite.

Acknowledgements

This work was financially supported by the Special Funds for the National Natural Science Foundation of China (No. U1608254), and the National Key R&D Program of China (No. 2018YFC1902002).

References

[1] Y.Q. Zhao, *Treatment of Copper Oxide Ore*, The Metallurgical Industry Press, Beijing, 1982.

[2] O.N. Ata, S. Çolak, Z. Ekinci, and M. Çopur, Determination of the optimum conditions for leaching of malachite ore in H_2SO_4 solutions, *Chem. Eng. Technol.*, 24(2001), No. 4, p. 409.

[3] J.S. Deng, S.M. Wen, Q. Yin, D.D. Wu, and Q.W. Sun, Leaching of malachite using 5-sulfosalicylic acid, *J. Taiwan Inst. Chem. Eng.*, 71(2017), p. 20.

[4] D. Bingöl and M. Canbazoğlu, Dissolution kinetics of malachite in sulphuric acid, *Hydrometallurgy*, 72(2004), No. 1-2, p. 159.

[5] D. Bingöl, M. Canbazoğlu, and S. Aydoğan, Dissolution kinetics of malachite in ammonia/ammonium carbonate leaching, *Hydrometallurgy*, 76(2005), No. 1-2, p. 55.

[6] A. Künkül, M.M. Kocakerim, S. Yapici, and A. Demirbağ, Leaching kinetics of malachite in ammonia solutions, *Int. J. Miner. Process.*, 41(1994), No. 3-4, p. 167.

[7] X. Wang, Q.Y. Chen, H.P. Hu, Z.L. Yin, and Z.L. Xiao, Solubility prediction of malachite in aqueous ammoniacal ammonium chloride solutions at 25°C, *Hydrometallurgy*, 99(2009), No. 3-4, p. 231.

[8] K.B. Fu, H. Lin, Y.B. Dong, X.L. Mo, and H. Wang, The rules of bacteria in malachite leaching of low acidity, *Met. Mine*, 40(2011), No. 3, p. 69.

[9] R.J. Ma, New development of hydrometallurgy, *Hydrometall. China*, 26(2007), No. 1, p. 1.

[10] K. Tkáčová, P. Baláž, B. Mišura, V.E. Vigdergauz, and V.A. Chanturiya, Selective leaching of zinc from mechanically activated complex Cu Pb Zn concentrate, *Hydrometallurgy*, 33(1993), No. 3, p. 291.

[11] C. Zhang, *Study on Mechanochemical Calorimeter and Mechanochemical Energy* [Dissertation], Central South University, Changsha, 2008.

[12] P. Baláž, Influence of solid state properties on ferric chloride leaching of mechanically activated galena, *Hydrometallurgy*, 40(1996), No. 3, p. 359.

[13] P. Baláž, *Extractive Metallurgy of Activated Minerals*, Elsevier, Amsterdam, 2000.

[14] D. Tromans and J.A. Meech, Enhanced dissolution of minerals: microtopography and mechanical activation, *Miner. Eng.*, 12(1999), No. 6, p. 609.

[15] N.J. Welham, Enhanced dissolution of tantalite/columbite following milling, *Int. J. Miner. Process.*, 61(2001), No. 3, p. 145.

[16] P. Baláž, *Mechanochemistry in Nanoscience and Minerals Engineering*, Springer, Berlin, Heidelberg, 2008.

[17] M.W. Gao, R.J. Holmes, and J. Pease, The latest developments in fine and ultrafine grinding technologies, [in] *23rd International Mineral Processing Congress*, Istanbul, 2006, p. 30.

[18] P. Baláž, M. Baláž, O. Shpotyuk, P. Demchenko, M. Vlček, M. Shopska, J. Briančin, Z. Bujňáková, Y. Shpotyuk, B. Selepová, and L. Balážová, Properties of arsenic sulphide (β-As_4S_4) modified by mechanical activation, *J. Mater. Sci.*, 52(2017), No. 3, p. 1747.

[19] R.A. Kleiv and M. Thornhill, The effect of mechanical activation in the production of olivine surface area, *Miner. Eng.*, 89(2016), p. 19.

[20] K. Tkáčová and N. Stevulová, Change in structure and enthalpy of carbonates and quartz accompanying grinding in air and aqueous environments, *Powder Technol.*, 52(1987), No. 2, p. 161.

[21] T. Tunç and K. Yildiz, Structural alterations in mechanically activated malachite, *Acta Phys. Pol. A*, 125(2014), No. 2, p. 177.

[22] G.R. Wang, H.Y. Yang, L.L. Tong, and Y.Y. Liu, Research on process mineralogy of oxidized copper ore in Luanshya, Zambia, *J. Northeastern Univ. Nat. Sci.*, 40(2019), No. 3, p. 350.

[23] R. Mejdoub, H. Hammi, M. Khitouni, J.J. Suñol, and A. M'nif, The effect of prolonged mechanical activation duration on the reactivity of portland cement: Effect of particle size and crystallinity changes, *Constr. Build. Mater.*, 152(2017), p. 1041.

[24] S. Romeis, J. Schmidt, and W. Peukert, Mechanochemical aspects in wet stirred media milling, *Int. J. Miner. Process.*, 156(2016), p. 24.

[25] P. Pourghahramani, E. Altin, M.R. Mallembakam, W.

Peukert, and E. Forssberg, Microstructural characterization of hematite during wet and dry millings using rietveld and xrd line profile analyses, *Powder Technol.*, 186(2008), No. 1, p. 9.

[26] S.M. Ohlberg and D.W. Strickler, Determination of percent crystallinity of partly devitrified glass by X-ray diffraction, *J. Am. Ceram. Soc.*, 45(1962), No. 4, p. 170.

[27] J.A. Goldsmith and S.D. Ross, The infra-red spectra of azurite and malachite, *Spectrochim. Acta Part A*, 24(1968), No. 12, p. 2131.

[28] M. Descamps and J.F. Willart, Perspectives on the amorphization/milling relationship in pharmaceutical materials, *Adv. Drug Delivery Rev.*, 100(2016), p. 51.

[29] P. Baláž, E. Turianicová, M. Fabián, R.A. Kleiv, J. Briančin, and A. Obut, Structural changes in olivine (Mg. Fe)$_2$SiO$_4$ mechanically activated in high-energy mills, *Int. J. Miner. Process.*, 88(2008), No. 1-2, p. 1.

[30] T. Tunç, F. Apaydin, and K. Yildiz, Effects of mechanical activation on the structure of nickeliferous laterite, *Acta Phys. Pol. A*, 123(2013), No. 2, p. 349.

[31] Y.J. Wang, S.L. Pan, X.L. Hou, G. Liu, J.D. Wang, and D.Z. Jia, Non-centrosymmetric sodium borate: Crystal growth, characterization and properties on $Na_2B_4O_{12}H_{10}$, *Solid State Sci.*, 12(2010), No. 10, p. 1726.

[32] Z. He, J. Zhou, Z.P. Lai, L.H. Yang, J.M. Liang, H. Long, and X.J. Ou, Quartz OSL dating of sand dunes of Late Pleistocene in the Mu Us Desert in northern China, *Quat. Geochronol.*, 5(2010), No. 2-3, p. 102.

[33] E. Horváth, R.L. Frost, É. Makó, J. Kristóf, and T. Cseh, Thermal treatment of mechanochemically activated kaolinite, *Thermochim. Acta*, 404(2003), No. 1-2, p. 227.

[34] R.L. Frost, W.N. Martens, L. Rintoul, E. Mahmutagic, and J.T. Kloprogge, Raman spectroscopic study of azurite and malachite at 298 and 77 K, *J. Raman Spectrosc.*, 33(2002), No. 4, p. 252.

[35] Y.Z. Xu, T. Jiang, M. Zhou, J. Wen, W.Y. Chen, and X.X. Xue, Effects of mechanical activation on physicochemical properties and alkaline leaching of boron concentrate, *Hydrometallurgy*, 173(2017), p. 32.